Electronic stopping of protons in magnesium from first principles

Chang-Kai Li,[1] Yang Liu,[2] Jian-Ming Xue,[1,*] Xiao-Ping OuYang,[2,3] and Feng-Shou Zhang[3,4,5]

[1]*State Key Laboratory of Nuclear Physics and Technology, School of Physics, Peking University, Beijing 100871, People's Republic of China*

[2]*School of Nuclear Science and Engineering, North China Electric Power University, Beijing 102206, People's Republic of China*

[3]*The Key Laboratory of Beam Technology and Material Modification of Ministry of Education, College of Nuclear Science and Technology, Beijing Normal University, Beijing 100875, People's Republic of China*

[4]*Beijing Radiation Center, Beijing 100875, People's Republic of China*

[5]*Center of Theoretical Nuclear Physics, National Laboratory of Heavy Ion Accelerator of Lanzhou, Lanzhou 730000, People's Republic of China*

(Received 31 October 2023; accepted 8 January 2024; published 26 January 2024)

The electronic energy loss rate from an energetic proton to electrons of an alkali metal magnesium (Mg) is investigated using real-time time-dependent density functional theory. Nonequilibrium simulations under various impact geometries are conducted to elucidate the role of the impact parameter in the dissipation mechanism. Unlike electronic stopping, which is significantly underestimated under channeling trajectories in the velocity regime around and above the stopping maximum, the predicted electronic stopping along the off-channeling trajectory, which explicitly accounts for the occasionally strong interaction with tightly bound inner-shell electrons, demonstrates quite satisfactory agreement with the experimental data throughout the velocity regime considered. This suggests that the impact parameter plays a crucial role when inner-shell excitation is concerned. Moreover, we conduct a quantitative analysis of the effect of the impact parameter on the electronic excitation in specific bands. An important conclusion drawn is that reducing the impact parameter significantly increases the intensity of the inner-shell excitation, especially for regimes around and above the stopping maximum, and it would also shift the excitation threshold to a lower velocity.

DOI: 10.1103/PhysRevA.109.012818

I. INTRODUCTION

The electronic energy loss of an irradiating ion in condensed matter is a fundamental quantity that governs the deposited heat, damage profile, and implantation depth. The physical characteristics of particle bombardment are essential issues in many modern technologies, including nuclear fission/fusion reactors [1,2], outer space exploration [3], medical ion therapy [4,5], ion implantation [6], material modification [7], and ion detection [8]. The electronic energy loss rate, a more general quantity, is defined as the kinetic energy lost per unit path length and has the dimensions of force. It is denoted as the stopping power, which consists of two components: the nuclear stopping power S_n resulting from elastic collisions with the nuclei of the target, and the electronic stopping power S_e attributed to the excitation of the electrons of the target. Notably, the ratio of inertia between the electron and nucleus is rather small, making the electron more responsive to impact. Consequently, in velocity regimes with electronic excitation significantly involved, the kinetic energy of the ion is predominantly lost electronically during the initial stages of collision.

Despite a long history, a comprehensive understanding of electronic stopping for all ion-solid collisions across all velocity regimes remains elusive. Light ion irradiation is relatively well understood, as the simple electronic configuration of the projectile allows for a focus on the underlying physical mechanisms involved in the target material excitation. Nevertheless, perhaps the most sophisticated investigation into electronic stopping resides in the velocity regime well above the target Fermi velocity, where the bound electrons on an irradiating ion are fully stripped [9,10], and the analytical models such as the Bethe-Bloch theory [11,12] and Lindhard-Winther theory [13] permit electronic stopping predictions with high accuracy.

In the regime of relatively low velocity, where electronic screening by bound electrons is concerned, the analytical models and their subsequent refinements [11–15] exhibit only limited applicability. This is attributed to their reliance on ambiguous parameters, such as the projectile charge or electron density, which not only possess multiple meaningful definitions but may also dynamically evolve during the projectile's transit [16]. The emergence of density functional theory (DFT) enables the direct extraction of key parameters, such as the electron density and screened potential, from first-principles theories in a self-consistent manner [17–20]. Notably, the recent advancement of time-dependent density functional theory (TDDFT) captures the transient nature of the electron density and screened potential during ion-target interactions [21–26].

In the early stages of the development of fully first-principles nonequilibrium TDDFT calculations for electronic stopping, significant efforts were dedicated to investigating

*Corresponding author. jmxue@pku.edu.cn

the electronic stopping of slow ions (with velocities below the Bohr velocity) [21,25,27–30]. The electronic excitations induced by slow ions predominantly arise from the weakly bound valence shell. In recent years, nonequilibrium TDDFT has also demonstrated a considerable potential to predict electronic stopping even for higher-velocity regimes around and above the stopping maximum [26,31–37], with the inclusion of deep-lying inner-shell configurations.

As the inner-shell excitation is involved, it becomes crucial to take the impact parameter into account, considering the localization of the core electron distribution. As per previous studies [34,35,38–40], in the high-velocity regime generally around and above the stopping maximum, the channeling impact geometry, which restricts the irradiating ion from closely interacting with the tightly bound host electrons, tends to underestimate the electronic stopping. Conversely, off-channeling geometry can consistently yield satisfactory results. Despite the importance of the impact parameter in electronic stopping with the inner-shell excitation concerned, quantitative *ab initio* research about the impact parameter dependence of the electronic excitation in a specific band is lacking.

In this article, we employ TDDFT in combination with Ehrenfest molecular dynamics (EMD) [41], to investigate the energy loss rate of a proton in magnesium (Mg) across a broad range of velocities. Additionally, we conduct a quantitative analysis of impact-parameter-dependent electron excitation in specific bands. Our primary objective is not only to provide an accurate prediction of the electronic stopping for protons in Mg but also to clarify the underlying physical mechanism by examining the influence of the impact parameter on electronic excitation. The remainder of this article is organized as follows: In Sec. II, we provide a brief overview of the theoretical framework and computational methods. Results are presented and discussed in Sec. III, where we focus on two main aspects: first, the presentation of the electronic stopping for various impact geometries in Sec. III A, and second, an in-depth discussion of the impact-parameter-dependent electronic excitation for a broad range of velocities in Sec. III B. Finally, conclusions are drawn in Sec. IV.

II. MODEL AND METHODS

During the course of the simulation, the energy transferred to the host electronic system from incident protons is monitored. For simplicity, and since the S_e is a velocity-resolved quantity, the intruder is constrained to move at a given velocity, and the excess in total system energy is used in determining the electronic stopping. First, a ground-state DFT calculation is performed to acquire the converged static state of the host Mg atoms and a doped hydrogen atom. Then in the TDDFT simulation, hydrogen ions are set to move with given velocities. The time-dependent Kohn-Sham (TDKS) equation describes the evolution of the electron density and energy of the system, due to the dynamics of effective single-particle states under the external potential generated by the incident and host nuclei. These states evolve in time with a self-consistent Hamiltonian that is a function of electron density $n(\vec{r}, t)$, using the approximated enforced time-reversal symmetry (AETRS) method [42]:

$$i\hbar\frac{\partial\varphi_i(\vec{r},t)}{\partial t} = \left\{-\frac{\hbar^2\nabla^2}{2m} - V_{\mathrm{KS}}[n(\vec{r},t)]\right\}\varphi_i(\vec{r},t). \quad (1)$$

Here, φ_i is the single-particle KS orbital evolving in the time-dependent effective potential V_{KS} which is a functional of the instantaneous electron density,

$$n(\vec{r},t) = \sum_{i=1}^{\mathrm{occ}} |\varphi_i(\vec{r},t)|^2. \quad (2)$$

The ionic motions of the target nuclei are neglected by fixing them in their equilibrium positions, given their velocity and movement are anticipated to experience only marginal changes during the transient interaction [43].

The simulations are performed using the OCTOPUS *ab initio* real-space code [44,45]. In this study, no basis set is employed. The external potential, electron density, and KS orbitals are discretized in a set of mesh grid points with a uniform spacing of 0.18 Å along the three spatial coordinates within the simulation box. Such mesh fineness corresponds to an energy cutoff of approximately 1160.59 eV in the plane-wave basis. A small time step of 0.001 fs is employed to ensure the stability of the time-dependent calculations. Using smaller time steps and grid spacings in simulations yields essentially identical results. The pseudopotential, specifically Mg10([core]$^2 2s^2 2p^6 3s^2$), with the K shell frozen in an ionic core and the other ten outer electrons explicitly included, is employed in this study. Such a practice makes no impact on the findings of this work, as the velocity regime considered is far from the excitation threshold of the $1s$ electrons. Both the projectile H and host Mg atoms in the present work are represented by scalar-relativistic nonlocal pseudopotentials, factorized in the Kleinman-Bylander form [46].

Periodic boundary conditions, in conjunction with the Ewald summation method [47,48], are employed throughout this study. A $4 \times 4 \times 4$ supercell consisting of 128 Mg atoms is selected to represent the target size. The lattice parameters used in this work are $a = b = 3.21$ Å, $c = 5.21$ Å, $\alpha = \beta = 90^\circ$, $\gamma = 120^\circ$, identical to the experimental values [49]. Only a single k point (Γ) is employed for the integration of the Brillouin zone.

The electronic stopping calculations using TDDFT are conducted for both channeling and off-channeling geometries. For the channeling scenarios, the center channeling as well as the "centroid" channeling proposed in Refs. [32,36,50] are adopted. In the off-channeling scenario, the projectile adopts a random trajectory direction within the host crystal, yielding an occasionally strong interaction between the projectile and the tightly bound electrons of the host atoms. Instead of calculating a classical ensemble average of projectile trajectories, a single long simulation as suggested by Schleife [35] is employed, which explores a wide range of impact parameters and thus densities. A "random direction" [0.543,0.313,0.779] (given normalized here) that is incommensurate with the crystal directions is utilized.

The key parameter S_e is extracted by performing a linear fit on the increase in total system energy. The evolution of the increase in the total energy of the system with a displacement

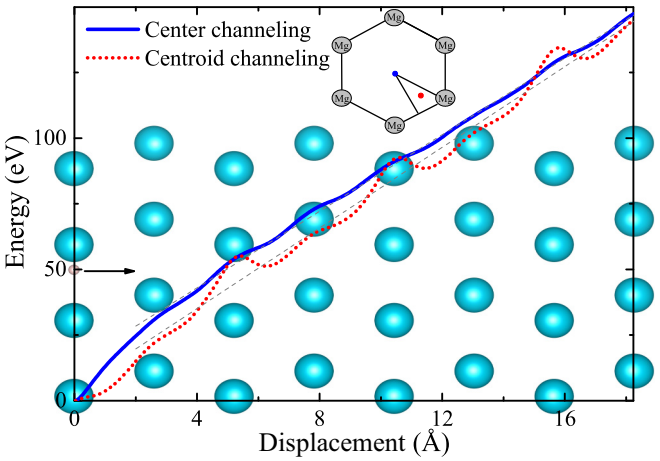

FIG. 1. The increase in the total energy of the system due to channeling protons with a velocity of 1.0 a.u. as a function of projectile displacement along the center and centroid trajectories in the ⟨100⟩ channel. The upper inset displays a sketch of the center and centroid trajectories (denoted by blue and red points, respectively). The centroid trajectory denotes the channeling along the centroid of a triangle formed by the center of the channel, an edge atom of the channel, and the midpoint between the edge atom and the adjacent edge atom. The lower inset illustrates the atom layers along the ⟨100⟩ direction.

of the projectile for channeling and off-channeling trajectories is presented in Figs. 1 and 2, respectively. To mitigate the influence of the wake potential induced by the reentry of the simulation cell along the same trajectory, the channeling S_e data are extracted by a linear fitting of the increase in the total system energy within one times a supercell thickness of about 17.1 Å, from which a kink with a length of 2 Å induced by the sudden movement at the beginning of the TDDFT simulation is removed.

For off-channeling geometry, the projectile does not reenter the simulation cell on the same trajectory each time, resulting in less influence from the wake potential compared to the channeling geometry. The calculated S_e for the off-channeling case is extracted by a linear fitting of the increase

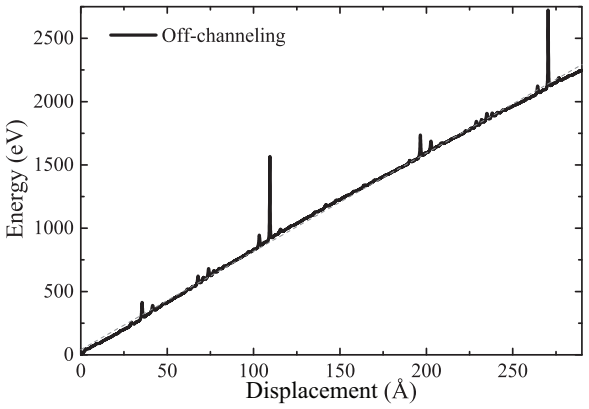

FIG. 2. The increase in the total energy of the system due to protons with a velocity of 1.0 a.u. as a function of the projectile's displacement along the off-channeling trajectory.

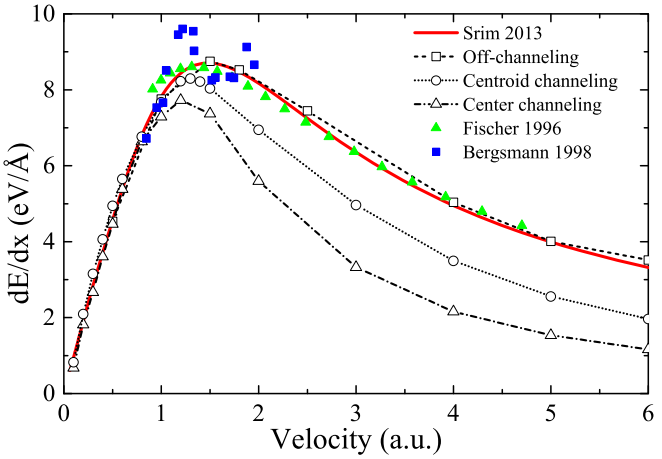

FIG. 3. Electronic stopping for center and centroid channeling (black open triangles and circles), as well as off-channeling protons (black open squares) as a function of velocity, together with the stopping and range of ions in matter (SRIM-2013) predictions (red solid line), and experimental data (solid symbols) by Fischer [51] and Bergsmann [52].

in the total system energy over a long trajectory spanning about 290 Å. The peaks in Fig. 2 represent close encounters with the host nuclei, and their magnitudes reflect the proximity between the projectile and host nuclei. As shown, the off-channeling geometry explores a significantly larger range of impact parameters compared to the channeling geometry, ensuring the randomness of the ion track to a large extent.

III. RESULTS AND DISCUSSION

A. Electronic stopping for random and channeling impact geometries

We present in Fig. 3 the simulated S_e results for the motion of proton in the velocity regime 0.1–6.0 a.u. along both the center and centroid channeling, as well as the off-channeling trajectories. The experimental data by Fischer [51] and Bergsmann [52] are also presented for comparison. It can be seen that for all impact geometries, the calculated results exhibit excellent agreements with the experimental data within the velocity regime below $v < 1.0$ a.u. As reported by Ullah *et al.* [21], in the low-velocity regime the impact parameter has a minor influence on the electronic energy loss, except for very slight impact parameters where the ion trajectory closely passes the host atoms. The agreement between the calculated results in the low-velocity regime for the center and centroid channeling trajectories, where close collisions with the host atoms are avoided, corroborates the conclusion drawn by Ullah *et al.* [21].

As the impact velocity increases, the S_e value for center channeling begins to underestimate the experimental data, with the simulated result being approximately 61% lower than the experimental data at $v = 5.0$ a.u.. For centroid channeling, the agreement between the calculated results and experimental data extends nearly up to the stopping maximum, which validates the legitimacy of the "centroid" impact geometry in velocity regimes below the stopping maximum. However, beyond the stopping maximum, the calculated results for the

"centroid" impact geometry also significantly underestimate the experimental data, with the simulated result being approximately 36% lower than the experimental data at $v = 5.0$ a.u.

For the off-channeling geometry, the calculated results for the velocity regime above the stopping maximum show a significant improvement, and there is excellent agreement with experimental data throughout the velocity regime considered. This indicates the occasional strong interaction with the tightly bound inner-shell electron contributes significantly to the electronic stopping in the high-velocity regime. According to the reports by Lohmann and collaborators [53–55], the enhancement in electronic stopping for off-channeling impact geometry can be attributed to the higher charge states due to the reionization of the captured electron on the projectile and also electron promotion, that only occurs in close interactions with the host atoms.

From the above analysis, we conclude that, in contrast to the low-velocity regime, the impact parameter plays a crucial role in determining the electronic stopping in the high-velocity regime. To illustrate this point quantitatively, we investigate the impact-parameter-dependent electronic excitation in the target in the following section.

B. Impact-parameter-dependent electronic excitation

Here, we demonstrate the electronic excitation in a specific band for ion-solid collisions under channeling conditions, employing five distinct impact parameters. First, we compute the time-dependent occupation of electronic states $C_{\rm occ}$, which is derived by projecting all time-dependent Kohn-Sham wave functions $\psi_n(t)$ onto the ground-state Kohn-Sham orbitals φ_i as [27,56]

$$C_{\rm occ}(\varepsilon_i) = \sum_n |\langle\varphi_i|\psi_n(t)\rangle|^2, \tag{3}$$

where ε_i is the eigenvalue of φ_i. Then, the total number of excited electrons is obtained as

$$N = \sum_i^{\varepsilon_i<E_{\rm F}} [O_{\rm occ}(\varepsilon_i) - C_{\rm occ}(\varepsilon_i)]\delta(\varepsilon - \varepsilon_i), \tag{4}$$

where $O_{\rm occ}(\varepsilon_i)$ is the occupation of the ground-state Kohn-Sham orbitals φ_i.

Under varying impact parameter conditions, we examine the velocity-resolved number of electrons excited from the valence $3s$ band, as well as from the low-lying $2p$ and $2s$ bands. They are derived by subtracting the ground-state occupation distribution from the occupied state distribution after the projectile passing through the length of one times of the supercell length along the ⟨100⟩ direction, according to Eq. (4). The results for specific band excitation are presented in Fig. 4. As observed in Fig. 4(a), in the low-velocity regime below $v < 1.0$ a.u., the electronic excitation in the valence $3s$ band exhibits minor differences for different impact geometries. This finding is consistent with the electronic stopping of the center and centroid channeling geometries that, with varied but relatively large impact parameters, exhibits a similar magnitude. However, for the low-impact parameters (trajectories 1 and 2) shown in Figs. 4(b) and 4(c), the inner-shell excitations are pronounced even in the low-velocity regime, and such a result corroborates the report by Ullah *et al.* [21] that in the low-velocity regime the impact parameter only plays a minor role, except at a very low-impact parameter.

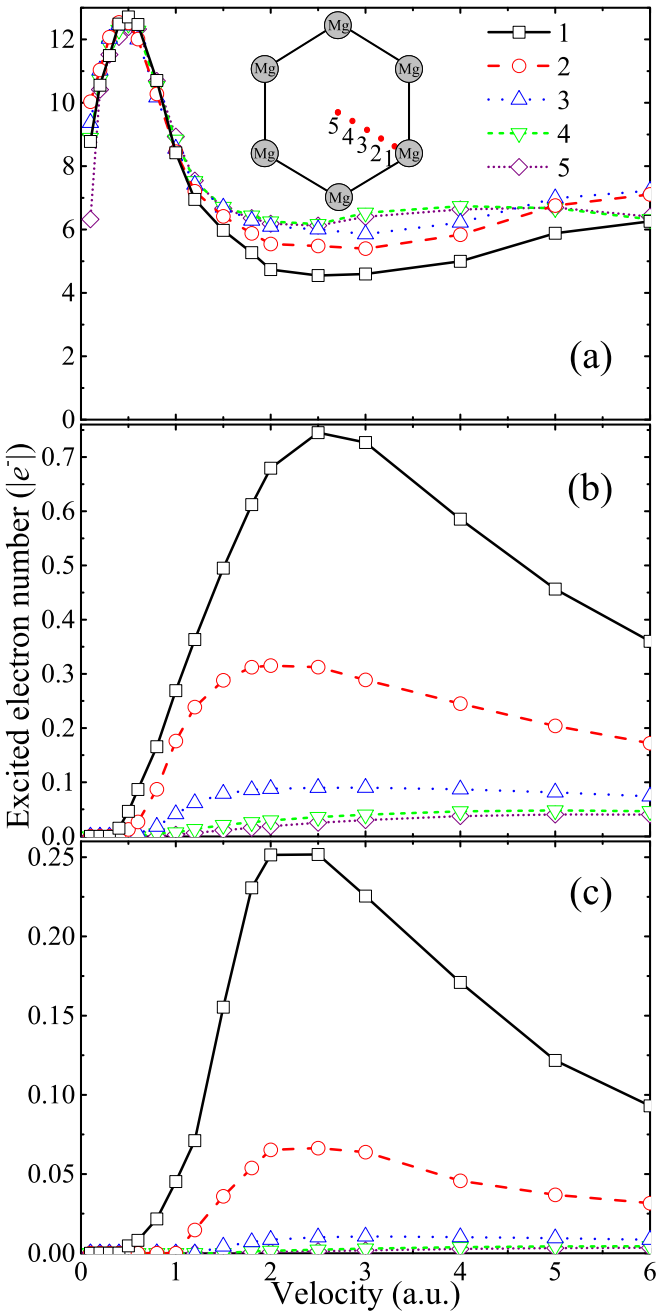

FIG. 4. Velocity-resolved number of excited $3s$, $2p$, and $2s$ electrons [shown in (a)–(c), respectively] after an ion-target collision with different impact parameters. The inset depicts the schematic of the employed impact geometries, wherein we adopt five trajectories with equal spacing from the center of the ⟨100⟩ channel to the edge atom's position. The impact parameters for trajectories 1–5 are 0.3706, 0.7412, 1.1118, 1.4824, and 1.8530 Å, respectively.

In the high-velocity regime, the excitations in the valence band decrease due to a significant reduction in interaction time [57]. However, there is a pronounced enhancement for the excitation in the deep-lying $2p$ and $2s$ bands, particularly for collisions with very low-impact parameters. This can be rationalized by the fact that electrons in specific shells can

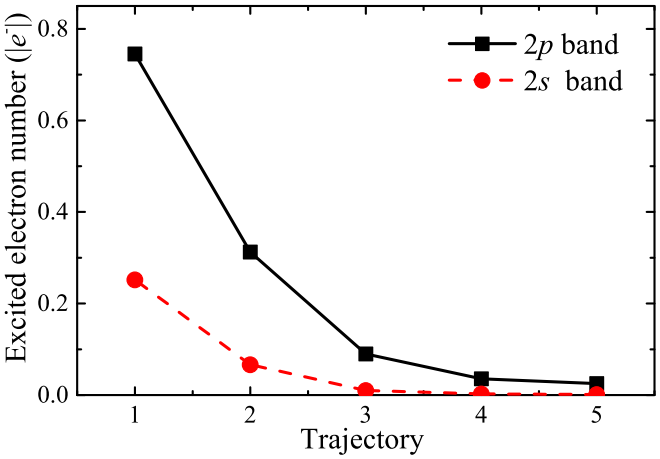

FIG. 5. Trajectory-dependent number of excited $2p$ and $2s$ electrons for a projectile with a velocity of $v = 2.5$ a.u.

only be effectively excited when the projectile approaches the average electronic velocity in this shell [58].

To depict the trend of impact-parameter-dependent inner-shell excitation, we demonstrate in Fig. 5 the number of $2p$ and $2s$ electrons excited in ion-target collisions with different impact parameters for a projectile with a velocity of 2.5 a.u. Significant attenuation in the excitation of $2p$ and $2s$ electrons can be found as the impact parameter increases, and such a result is consistent with the finding in our previous work that an inner-shell excitation is quite a localized phenomenon, and it can only occur when the projectile encounters host nuclei that are close enough [59]. For instance, the magnitude of $2p$ excitation at a velocity of 2.5 a.u for trajectory 1 decreases to 45% at trajectory 2, and trajectory 4 only accounts for 8% of that of trajectory 1. This result indicates that the inner-shell excitation is intimately related to the impact geometry and the efficiency increases sharply with the decrease of the impact parameter. Regarding the contributions of specific band excitations to the electronic stopping in the high-velocity regime, although the valence $3s$ band excitation is dominant, the excitation of deep-lying $2p$ and $2s$ bands is also pronounced in low-impact parameter scenarios. Particularly, the energies dissipated during the excitation of deep-lying $2p$ and $2s$ bands are much higher than that of a valence band, making them indispensable in determining electronic stopping.

From the above discussion, it can be concluded that inner-shell excitation is crucial in the high-velocity regime, and it can only be effectively activated under low-impact parameter conditions. Considering the collision simulations for the center and centroid channeling impact geometries, which with relatively large impact parameters, overlook the excitation tightly bound inner-shell electron to a large extent, we find they would inevitably underestimate the electronic stopping in a high-velocity regime. Conversely, off-channeling, which captures the close interaction between the projectile and deep-lying electrons, achieves a rather good agreement with experimental data.

It is noted that no threshold is observed for valence-band excitations, so this result is anticipated given the absence of a band gap for metal Mg, while for deep-lying $2p$ and $2s$ band excitation, impact-parameter-dependent thresholds are found. We estimate the electronic excitation thresholds of the deep-lying $2p$ and $2s$ configurations through the method suggested in Ref. [38],

$$v_{\mathrm{th}} = \frac{\Delta E}{2\hbar k_{\mathrm{F}}}, \tag{5}$$

where ΔE represents the offset of the specific band, which corresponds to the interval between the up edge of the specific band and the Fermi energy level of Mg. The Fermi wave vector can be quantified as $k_{\mathrm{F}} = 1.92/r_s$, where $r_s = 1.34$ a.u. for the effective uniform electron gas encompassing the valence $3s$ electrons of Mg. Based on the above equation, we estimate the velocity threshold for $2p$ and $2s$ bands with $\Delta E = 32$ and 71 eV, respectively, at $v_{\mathrm{th}} = 0.82$ and 1.71 a.u., respectively.

Based on the results of TDDFT simulations presented in Figs. 4(b) and 4(c), the thresholds for relatively large impact parameters (trajectories 4 and 5) are close to the values predicted by Eq. (5) for both $2p$ and $2s$ band excitations. However, for low-impact parameters, the predicted thresholds by TDDFT are notably lower than that predicted by Eq. (5). For this, we interpret that other electronic processes, which go beyond direct excitation, such as a shift in the band structure and charge exchange, are involved in collisions with very low impact parameters.

IV. CONCLUSIONS

We report theoretical research from first principles of the nonadiabatic interaction of a proton with Mg in a wide range of velocities for various impact geometries. Electronic stopping under channeling impact geometries, which overlooks the excitation of tightly bound inner-shell electrons to a large extent, is found to significantly underestimate the experimental data in the high-velocity regime. However, the simulations along the off-channeling trajectory, which explicitly takes into account the occasionally strong interaction with tightly bound inner-shell electrons, reproduce the experimental data rather well throughout the velocity regime considered. These results suggest that the impact parameter plays a crucial role when inner-shell excitation is concerned. To elucidate this point, we conduct a quantitative analysis of the effect of impact parameter on the electronic excitation of a specific band. Our results reveal that, in the high-velocity regime, inner-shell excitation exerts a significant influence on the electronic stopping power, which can only be effectively activated at very low-impact parameters. Additionally, we observe that reducing the impact parameter shifts the excitation threshold to lower velocities. This work provides guidance for the accurate prediction of electron stopping power and the rational design of experiments.

ACKNOWLEDGMENT

This work was supported by the National Natural Science Foundation of China under Grants No. 12105205 and No. 12135002, and China Postdoctoral Science Foundation (Grants No. 2019M662693, No. 2020T130486, and No. 2021M700003).

[1] T. Diaz de la Rubia, H. M. Zbib, T. A. Khraishi, B. D. Wirth, M. Victoria, and M. J. Caturla, Nature (London) **406**, 871 (2000).
[2] G. Ackland, Science **327**, 1587 (2010).
[3] X. Wang and J. R. Key, Science **299**, 1725 (2003).
[4] C. Bert, R. Engenhart-Cabillic, and M. Durante, Med. Phys. **39**, 1716 (2012).
[5] K. G. Reeves, Y. Yao, and Y. Kanai, Phys. Rev. B **94**, 041108(R) (2016).
[6] Y. Zhang, I.-T. Bae, K. Sun, C. Wang, M. Ishimaru, Z. Zhu, W. Jiang, and W. J. Weber, J. Appl. Phys. **105**, 104901 (2009).
[7] H. Kraus, D. Simin, C. Kasper, Y. Suda, S. Kawabata, W. Kada, T. Honda, Y. Hijikata, T. Ohshima, V. Dyakonov *et al.*, Nano Lett. **17**, 2865 (2017).
[8] R. Rando, A. Bangert, D. Bisello, A. Candelori, P. Giubilato, M. Hirayama, R. Johnson, H.-W. Sadrozinski, M. Sugizaki, J. Wyss, and M. Ziegler, IEEE Trans. Nucl. Sci. **51**, 1067 (2004).
[9] J. Knipp and E. Teller, Phys. Rev. **59**, 659 (1941).
[10] P. Sigmund, Phys. Rev. A **56**, 3781 (1997).
[11] H. Bethe, Ann. Phys. **397**, 325 (1930).
[12] F. Bloch, Ann. Phys. **408**, 285 (1933).
[13] J. Lindhard and A. Winther, K. Dan. Vidensk. Selsk., Mat.-Fys. Medd. **34**, 14 (1964).
[14] N. Bohr and J. Lindhard, K. Dan. Vidensk. Selsk., Mat.-Fys. Medd. **1**, 28 (1954).
[15] G. Iafrate and J. Ziegler, J. Appl. Phys. **50**, 5579 (1979).
[16] I. Abril, R. Garcia-Molina, C. D. Denton, F. J. Pérez-Pérez, and N. R. Arista, Phys. Rev. A **58**, 357 (1998).
[17] E. Runge and E. K. U. Gross, Phys. Rev. Lett. **52**, 997 (1984).
[18] P. M. Echenique, R. M. Nieminen, J. C. Ashley, and R. H. Ritchie, Phys. Rev. A **33**, 897 (1986).
[19] A. Arnau, M. Peñalba, P. M. Echenique, F. Flores, and R. H. Ritchie, Phys. Rev. Lett. **65**, 1024 (1990).
[20] E. K. U. Gross and W. Kohn, Phys. Rev. Lett. **55**, 2850 (1985).
[21] R. Ullah, F. Corsetti, D. Sánchez-Portal, and E. Artacho, Phys. Rev. B **91**, 125203 (2015).
[22] M. Caro, A. Tamm, A. Correa, and A. Caro, J. Nucl. Mater. **507**, 258 (2018).
[23] C.-K. Li, S. Liu, Q. Cao, F. Wang, X.-P. OuYang, and F.-S. Zhang, Phys. Rev. A **100**, 052707 (2019).
[24] A. Lim, W. M. C. Foulkes, A. P. Horsfield, D. R. Mason, A. Schleife, E. W. Draeger, and A. A. Correa, Phys. Rev. Lett. **116**, 043201 (2016).
[25] J. M. Pruneda, D. Sánchez-Portal, A. Arnau, J. I. Juaristi, and E. Artacho, Phys. Rev. Lett. **99**, 235501 (2007).
[26] R. Ullah, E. Artacho, and A. A. Correa, Phys. Rev. Lett. **121**, 116401 (2018).
[27] M. A. Zeb, J. Kohanoff, D. Sánchez-Portal, A. Arnau, J. I. Juaristi, and E. Artacho, Phys. Rev. Lett. **108**, 225504 (2012).
[28] F. Mao, C. Zhang, J. Dai, and F.-S. Zhang, Phys. Rev. A **89**, 022707 (2014).
[29] C.-K. Li, F. Wang, B. Liao, X.-P. OuYang, and F.-S. Zhang, Phys. Rev. B **96**, 094301 (2017).
[30] C.-K. Li, F. Mao, F. Wang, Y.-L. Fu, X.-P. Ouyang, and F.-S. Zhang, Phys. Rev. A **95**, 052706 (2017).
[31] A. A. Shukri, F. Bruneval, and L. Reining, Phys. Rev. B **93**, 035128 (2016).
[32] D. C. Yost, Y. Yao, and Y. Kanai, Phys. Rev. B **96**, 115134 (2017).
[33] Y. Yao, D. C. Yost, and Y. Kanai, Phys. Rev. Lett. **123**, 066401 (2019).
[34] C.-W. Lee, J. A. Stewart, R. Dingreville, S. M. Foiles, and A. Schleife, Phys. Rev. B **102**, 024107 (2020).
[35] A. Schleife, Y. Kanai, and A. A. Correa, Phys. Rev. B **91**, 014306 (2015).
[36] A. Ojanperä, A. V. Krasheninnikov, and M. Puska, Phys. Rev. B **89**, 035120 (2014).
[37] E. E. Quashie and A. A. Correa, Phys. Rev. B **98**, 235122 (2018).
[38] E. E. Quashie, B. C. Saha, and A. A. Correa, Phys. Rev. B **94**, 155403 (2016).
[39] X.-D. Zhao, F. Mao, S.-M. Li, B.-S. Li, H. Mao, F. Wang, and F.-S. Zhang, Phys. Rev. A **104**, 032801 (2021).
[40] W.-Q. Zuo, F. Mao, S.-M. Li, W.-Q. Jin, R.-D. Chen, G.-G. Xiong, C.-Z. Gao, F. Wang, and F.-S. Zhang, Phys. Rev. A **107**, 012818 (2023).
[41] X. Andrade, A. Castro, D. Zueco, J. L. Alonso, P. Echenique, F. Falceto, and A. Rubio, J. Chem. Theory Comput. **5**, 728 (2009).
[42] A. Castro, M. A. L. Marques, and A. Rubio, J. Chem. Phys. **121**, 3425 (2004).
[43] A. A. Correa, J. Kohanoff, E. Artacho, D. Sánchez-Portal, and A. Caro, Phys. Rev. Lett. **108**, 213201 (2012).
[44] M. A. L. Marques, A. Castro, G. F. Bertsch, and A. Rubio, Comput. Phys. Commun. **151**, 60 (2003).
[45] A. Castro, H. Appel, M. Oliveira, C. A. Rozzi, X. Andrade, F. Lorenzen, M. A. L. Marques, E. K. U. Gross, and A. Rubio, Phys. Status Solidi B **243**, 2465 (2006).
[46] L. Kleinman and D. M. Bylander, Phys. Rev. Lett. **48**, 1425 (1982).
[47] I.-C. Yeh and M. L. Berkowitz, J. Chem. Phys. **111**, 3155 (1999).
[48] B. A. Wells and A. L. Chaffee, J. Chem. Theory Comput. **11**, 3684 (2015).
[49] M. Straumanis, J. Appl. Phys. **20**, 726 (1949).
[50] A. Kononov and A. Schleife, Nano Lett. **21**, 4816 (2021).
[51] P. Fischer, C. Eppacher, G. Höfler, and D. Semrad, Nucl. Instrum. Methods Phys. Res., Sect. B **115**, 27 (1996).
[52] M. Bergsmann, P. Hörlsberger, F. Kastner, and P. Bauer, Phys. Rev. B **58**, 5139 (1998).
[53] S. Lohmann, R. Holeňák, and D. Primetzhofer, Phys. Rev. A **102**, 062803 (2020).
[54] S. Lohmann and D. Primetzhofer, Phys. Rev. Lett. **124**, 096601 (2020).
[55] S. Lohmann, R. Holeňák, P. L. Grande, and D. Primetzhofer, Phys. Rev. B **107**, 085110 (2023).
[56] T. Otobe, M. Yamagiwa, J.-I. Iwata, K. Yabana, T. Nakatsukasa, and G. F. Bertsch, Phys. Rev. B **77**, 165104 (2008).
[57] C.-K. Li, J.-M. Xue, and F.-S. Zhang, Phys. Rev. A **106**, 022807 (2022).
[58] R. A. Lewis, G. A. Smith, and W. S. Toothacker, Phys. Rev. A **44**, 392 (1991).
[59] C.-K. Li, X. Guo, J.-M. Xue, and F.-S. Zhang, Phys. Rev. A **107**, 052814 (2023).